Journal of Fluids and Structures (1998) **12,** 1041–1053
Article No. fl980178

VORTEX SHEDDING RESONANCE FROM A ROTATIONALLY OSCILLATING CYLINDER

N. Fujisawa

Department of Mechanical and Production Engineering, Niigata University
8050 Ikarashi 2, Niigata, 950-2181, Japan

AND

K. Ikemoto, K. Nagaya

Department of Mechanical System Engineering, Gunma University
1-5-1 Tenjin, Kiryu, 376-8515, Japan

(Received 12 March 1998 and in revised form 24 August 1998)

Vortex shedding resonance of a circular cylinder wake to a forced rotational oscillation has been investigated experimentally by measuring the velocity fluctuations in the wake, pressure distributions over the cylinder surface, and visualizing the flow field with respect to cylinder oscillations. The vortex shedding resonance occurs near the natural shedding frequency at small amplitude of cylinder oscillations, while the peak resonance frequency shifts to a lower value with an increase in oscillation amplitude. The drag and lift forces acting on the cylinder at fixed forcing Strouhal number indicate that the phase lag of fluid forces to the cylinder oscillations increases with an increase in oscillation amplitude, supporting the variation of resonance frequency with oscillation amplitude. The comparative study of the measured pressure distributions and the simultaneous flow visualizations with respect to cylinder rotation shows the mechanisms of phase lag, which is due to the strengthened vortex formation and the modification of the surface pressure distributions.

1. INTRODUCTION

Vortex streets are formed in the wake of a bluff body over a wide range of Reynolds numbers. The appearance of vortex streets produces cyclic fluid forces acting on the cylinder. This interaction between the fluid and the bluff-body structure causes a flow-induced vibration, when the vortex shedding frequency is near the natural frequency of the bluff-body structure. A number of researchers have studied the effects of flow-induced and forced cylinder oscillations on the cylinder wake, the recent results of which are summarized in review papers by Bearman (1984), Naudascher (1987), Griffin & Hall (1991), and others. The literature covers the effect of cross-flow oscillations and in-line oscillations, but studies on the rotational oscillations are very few.

The effects of rotational oscillations on the cylinder wake were first studied by Okajima *et al.* (1975), who examined the response of the flow to rotational oscillations both numerically and experimentally. Later, Taneda (1978) visualized the flow around a rotationally oscillating cylinder in the laminar regime and demonstrated the possible suppression of the cylinder wake with an increase in forcing frequency. Recently, Filler *et al.* (1991) investigated the frequency response of the cylinder wake to small-amplitude rotational oscillations. It

0889–9746/98/081041 + 13 $30.00

was shown that rotational oscillations corresponding to cylinder peripheral speeds less than 3% of the free stream can influence the Karman mode of vortex generation. Tokumaru & Dimotakis (1991) investigated the flow at larger forcing frequencies than the natural one in a wide range of oscillation amplitude and at moderate Reynolds numbers. They indicated the possible suppression of vortex shedding and the corresponding reduction in the estimated drag forces at several times larger frequency than the natural shedding frequency, based on the flow visualization and the wake profile measurements. However, the flow structure and the fluid forces on the rotary oscillating cylinder especially near the resonance condition are not so well understood, in spite of its importance for application to the feedback control of vortex shedding (Fujisawa & Kawaji, 1995).

The purpose of this paper is to study the vortex shedding resonance of a rotationally oscillating cylinder at moderate Reynolds numbers. The velocity fluctuations in the wake and the pressure distributions over the cylinder are measured and flow visualizations with respect to cylinder rotation are conducted simultaneously to explore the mechanisms of vortex shedding resonance associated with rotary oscillations.

2. EXPERIMENTAL APPARATUS AND PROCEDURE

Figure 1 shows an illustration of the test-section in the present study. The coordinate system is chosen in such a way that the x-axis is along the flow direction, the y-axis is in the vertical direction, perpendicular to the flow, and the origin is located at the centre of the cylinder. The experiments are carried out in an open test-section of a return-circuit wind tunnel with the test-section of square cross-section 0·5 m × 0·5 m and 1·5 m in length, which provides a uniform velocity distribution. A smooth circular cylinder of radius 50 mm is positioned at 200 mm downstream from the entrance of the test-section, with its axis inclined to horizontal direction. The cylinder is supported by two vertical side walls of transparent material with dimensions of 0·5 m in width and 1·5 m in length. To minimize the end-effects of a circular cylinder, end-plates of radius 60 mm are fixed at the cylinder edges, and the

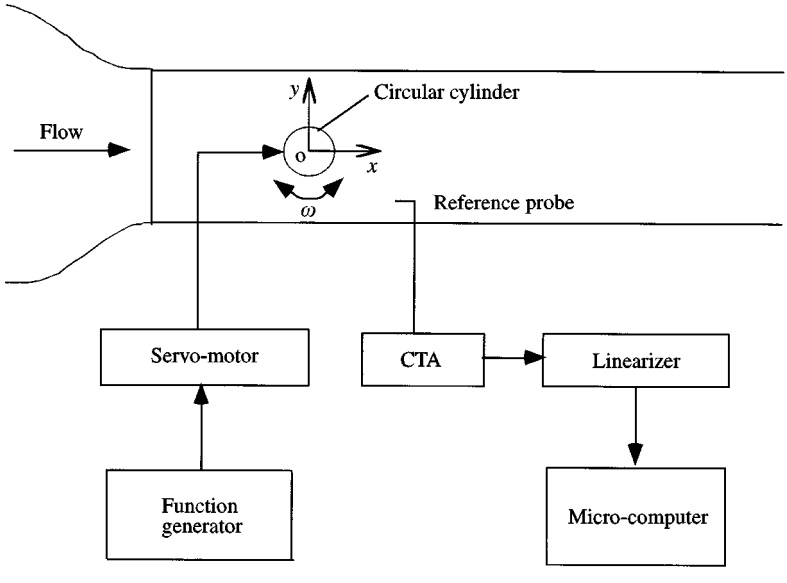

Figure 1. Experimental apparatus for rotationally oscillating circular cylinder.

clearance between the wall and the cylinder is kept small enough to allow smooth cylinder oscillations.

Preliminary measurements indicate that the velocity distribution at the cylinder location is uniform within an accuracy of 1% of the free-stream velocity in a spanwise distance of 400 mm. The free-stream velocity is estimated from the calibrated relation between the free-stream velocity at the test-section without the cylinder and the rotation rate of the blower. It is noted that the present experiment is carried out at an area blockage ratio of 0·2 and a cylinder aspect ratio of 5. Although they would affect the shedding frequency and the fluid forces on the cylinder to some extent (King 1977), these effects are not considered in the data analysis. However, the measurement of streamwise velocity distribution at the shear layer indicates a spanwise uniformity in the central 300 mm within an accuracy of 3% of the free-stream velocity. The rotation of the circular cylinder was achieved by using an AC servo motor located at the end of the cylinder. The other end of the cylinder was supported by a rotary bearing to have smooth rotation. The angular velocity of the cylinder was controlled to be proportional to the input voltage of the motor, which was supplied from a sine-wave generator. The AC servo motor allows the cylinder oscillations up to a frequency 8 Hz without significant phase lag between the input voltage and the measured angular velocity of the cylinder. However, the presence of the phase lag of the motor was considered in the present data analysis. It is noted that the maximum angle of rotary oscillation, θ_{max}, is smaller than 160°. Velocity fluctuations in the cylinder wake are detected by a hot-wire probe, which is located at $x/R = 3$ and $y/R = -1{\cdot}6$. Here, x and y are streamwise and normal coordinates measured from the centre of cylinder and R is the cylinder radius. The velocity signal is processed through a linearizer and analysed in a microcomputer fitted with AD converter.

Measurement of pressure distributions over the cylinder surface is carried out using an experimental arrangement as shown in Figure 2. A pressure hole of 1 mm in diameter is located on the centre plane of the cylinder, which is connected by a stainless-steel tube through a mechanical seal to a pressure transducer of strain-gauge type fixed outside the cylinder. The frequency response of the measuring system including the tubing is calibrated by the pulse input-signal and is found to be flat up to 200 Hz, which is high enough for the present measurment of phase-averaged pressure distributions. The output signal from the pressure transducer is analysed in the computer by sampling simultaneously the angular velocity signal of the servo-motor and the pulse signal from the photosensor for detecting

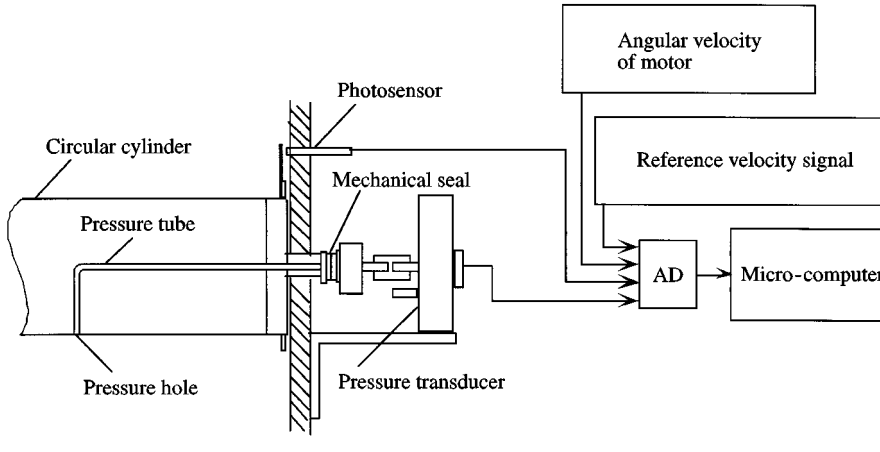

Figure 2. Experimental arrangement for measuring pressure over rotationally oscillating circular cylinder.

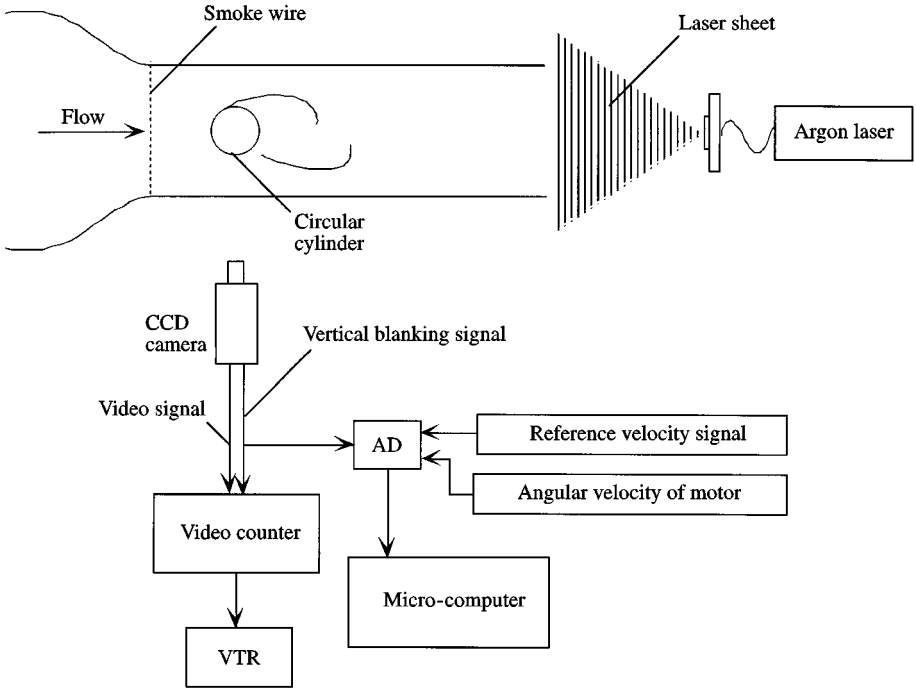

Figure 3. Experimental arrangement for visualizing the flow with respect to cylinder rotation.

the angular position of the pressure hole. After the data analysis with reference to the angular velocity signal of the motor, the phase-averaged pressure distributions over the cylinder surface with respect of the cylinder rotation are estimated. The measurement is carried out at the free-stream velocity $U = 3$ m/s, which corresponds to a Reynolds number $\mathrm{Re}(=2RU/\nu) = 2 \times 10^4$. The drag and lift forces are estimated by integrating the pressure distributions over the cylinder surface.

The flow field around the cylinder is visualized by the smoke-wire method. The experimental arrangement is shown in Figure 3. To facilitate the analysis of the flow and the cylinder motion, simultaneous data sampling of the angular velocity signal of the cylinder rotation is carried out at the same instant of flow observation. The angular velocity signal is acquired by a data sampling computer with AD converter, when an external trigger of the vertical blanking signal is supplied from a CCD camera for simultaneous data acquisition and analysis. A CCD camera, used for recording changes of the vortex formation, is connected to the VTR through a video counter and to the computer by a synchronous pulse from a CCD camera. The flow field is illuminated by an argon-ion laser sheet of 3 W, which has a thickness of 10 mm. The visualization experiment is carried out at the free-stream velocity $U = 1$ m/s.

3. RESULTS AND DISCUSSIONS

Figure 4 shows a typical trace of the angular velocity signal of the cylinder and the filtered reference velocity signal of the hot-wire probe, which is plotted against time, t. Here, the forcing Strouhal number $S_f(=2Rf/U)$ is set to 0·17 and the oscillation amplitude $V_r(=R\omega_{\max}/U) = 0{\cdot}38$, to keep a vortex shedding resonance, where R is the radius of circular cylinder, U the free-stream velocity, f the forcing frequency, $\omega_{\max}$ the maximum

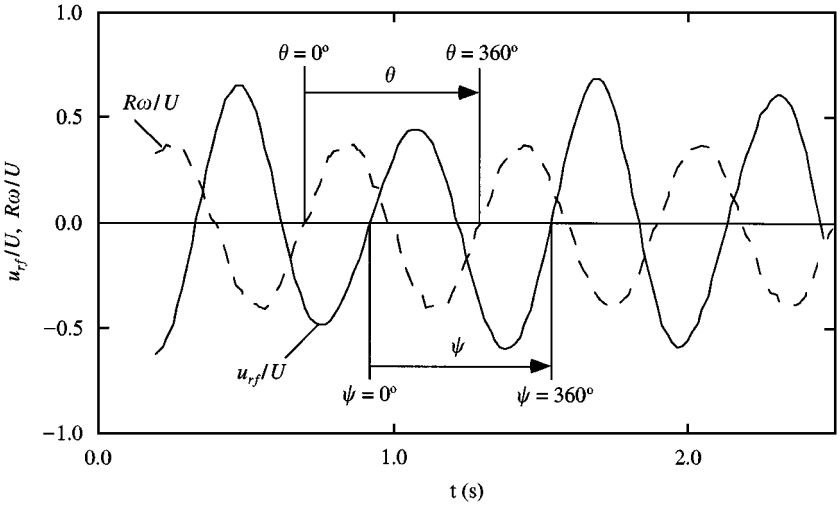

Figure 4. Example of angular velocity of cylinder oscillations and filtered reference velocity.

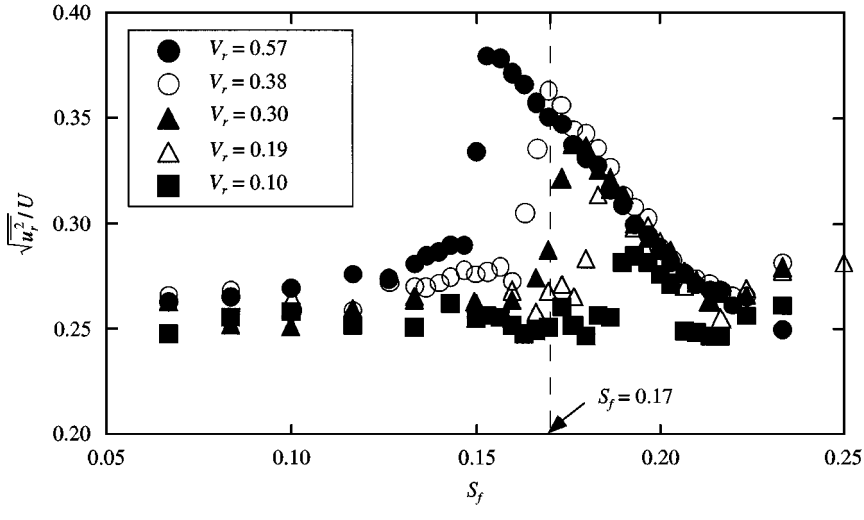

Figure 5. Response of reference velocity fluctuations to rotary cylinder oscillations.

angular velocity of cylinder rotation. The angular velocity is sinusoidal, and a positive angular velocity corresponds to a counterclockwise rotation of the cylinder set in a flow geometry as shown in Figure 1. Figure 4 also shows a definition of the oscillation angle θ of the rotary cylinder oscillations and the vortex angle ψ of the cylinder wake, which indicate cyclic angles measured from the transition of clockwise to counterclockwise cylinder rotation and that of negative to positive filtered velocity at the reference probe, respectively.

Figure 5 shows the response of the reference velocity fluctuations at the cylinder wake ($x/R = 3$ and $y/R = -1{\cdot}6$) to the imposed rotary oscillations of the cylinder. The forcing Strouhal numbers are varied in a range of $S_f = 0{\cdot}05$–$0{\cdot}25$ and the oscillation amplitude $V_r = 0{\cdot}1$–$0{\cdot}6$. It is clearly seen that the velocity fluctuations are strengthened near the natural frequency of vortex shedding ($S_r = 0{\cdot}2$), when the oscillation amplitude is small

$V_r \leq 0{\cdot}1$. As the oscillation amplitude V_r is increased, the reference velocity fluctuations are strengthened in magnitude, but the peak frequency of the response curve shifts to a smaller forcing Strouhal number. Therefore, the forcing frequency range in vortex shedding resonance tends to a smaller frequency as the oscillation amplitude becomes larger. A similar relation between the velocity fluctuation and forcing Strouhal number is also obtained at a lower free-stream velocity of $U = 1$ m/s, which is the case for the flow visualization experiment.

Figure 6(a, b) shows the variations of phase-averaged drag and lift coefficient $C_{D,\theta}$, $C_{L,\theta}$ with the oscillation angle θ at a fixed Strouhal number $S_r = 0{\cdot}17$, respectively, which are obtained by integrating the pressure distributions at the same oscillation angle θ of cylinder rotation. Here, the phase averaged drag coefficient is defined as $C_{D,\theta} = 2F_{x\theta}/\rho U^2 R$ and the corresponding lift coefficient is $C_{L,\theta} = 2F_{y\theta}/\rho U^2 R$, where $F_{x\theta}$ and $F_{y\theta}$ are the streamwise and normal forces in a unit length of cylinder at the oscillation angle θ, respectively. The experimental data cover a range of ocsillation amplitude $V_r = 0{\cdot}1$–$0{\cdot}38$. The drag coefficient has two peaks in one cycle of rotary oscillations of the cylinder, while the lift coefficient shows one peak, which agrees with the usual fluid force behavior acting on

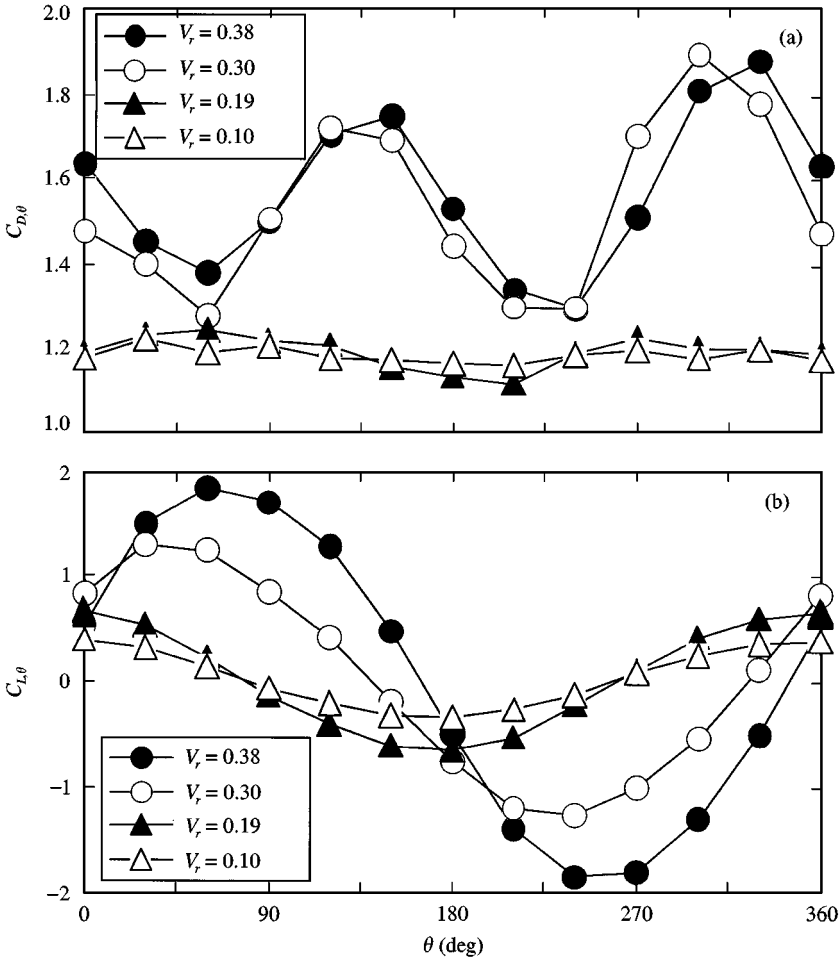

Figure 6. Variations of drag and lift forces with oscillation angle of cylinder at a forcing Strouhal number ($S_r = 0{\cdot}17$): (a) drag coefficient; (b) lift coefficient.

a stationary cylinder as observed by Drescher (1956). It is clearly seen that the magnitude of variation in drag and lift coefficient is greatly increased at the two larger oscillation amplitudes $V_r = 0{\cdot}30$ and $0{\cdot}38$. These changes in magnitude are well reproduced in the variations of velocity fluctuations along a line of constant forcing Strouhal number $S_r = 0{\cdot}17$ in Figure 5. Although the distributions of drag and lift coefficients at the two larger oscillation amplitudes look similar, the other results at smaller oscillation amplitudes $V_r = 0{\cdot}10$ and $0{\cdot}19$ show different features of distributions, that is the shift of the curve peaks to smaller oscillation angles. It should be noted that the delay in phase might be partly due to the increase in blockage, as the wake becomes larger.

Figure 7(a, b) shows the phase-averaged drag and lift coefficients in the peak resonance of vortex shedding, respectively, where the oscillation amplitudes are set to the same value as in Figure 6 but the forcing Strouhal numbers are slightly modified to have peak velocity fluctuations. Similar to an increase in peak velocity fluctuations with oscillation amplitude in Figure 5, the magnitude of drag and lift coefficients increases with an increase in oscillation amplitude, which appears even for the low V_r. The distributions of drag and lift

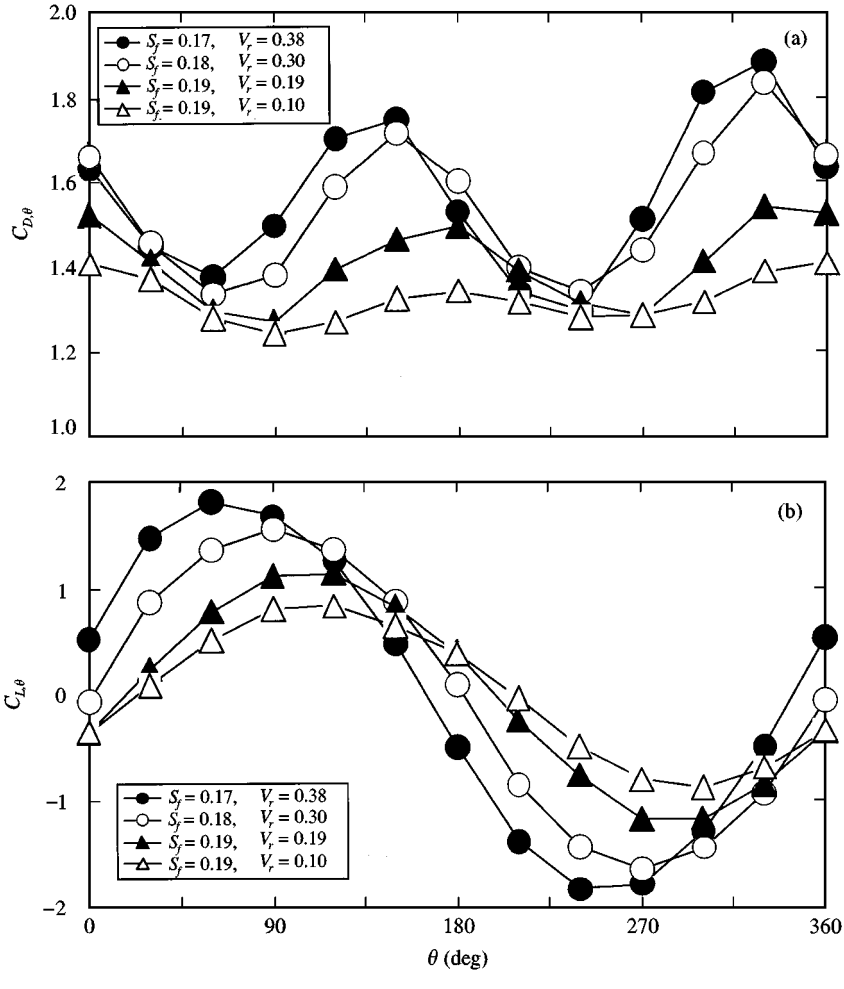

Figure 7. Variations of drag and lift forces with oscillation angle of cylinder at peak resonance of vortex shedding: (a) drag coefficient; (b) lift coefficient.

coefficient appear more similar in shape than those of the fixed Strouhal numbers in Figure 6, but there are still some phase variations in these distributions. This result suggests that the phase between the cylinder oscillation and the fluid forces acting on the cylinder varies with the oscillation amplitude and forcing Strouhal number. It can be considered from Figures 6 and 7 that the increase in the oscillation amplitude and the forcing Strouhal number results in increases in phase lag of the fluid forces to the cylinder oscillation.

Figure 8(a, b) shows the variations of phase-averaged drag and lift coefficient $C_{D,\theta}$, $C_{L,\theta}$ in the peak resonance of vortex shedding, which are plotted against the vortex angle ψ, respectively. The results for the stationary cylinder are also indicated here for comparison. It is clearly seen that both the drag and lift coefficients increase gradually with an increase in oscillation amplitude but the distributions are more similar in shape than those observed in Figure 7, which are plotted against oscillation angle θ. Figure 9 shows the pressure distributions and the corresponding flow visualization pictures at various oscillation angles $\theta = 0$, 90, 180 and 270° of the cylinder in peak resonance of vortex shedding, where the

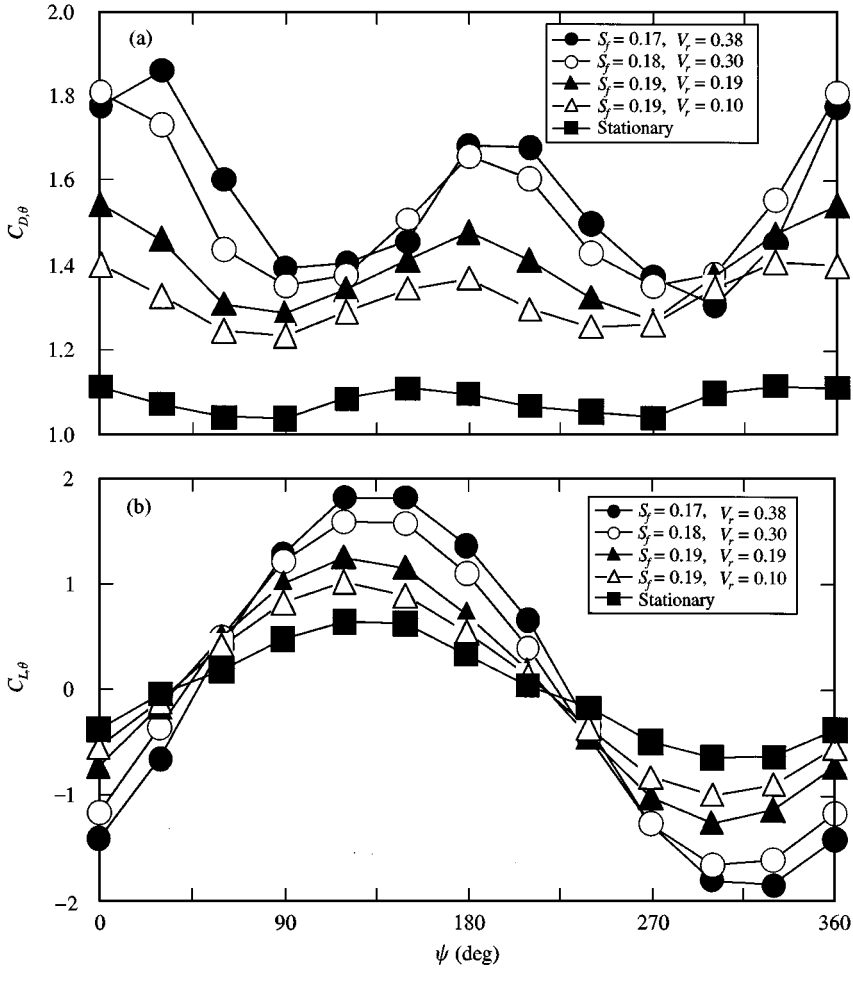

Figure 8. Variations of drag and lift forces with vortex angle at peak resonance of vortex shedding: (a) drag coefficient; (b) lift coefficient.

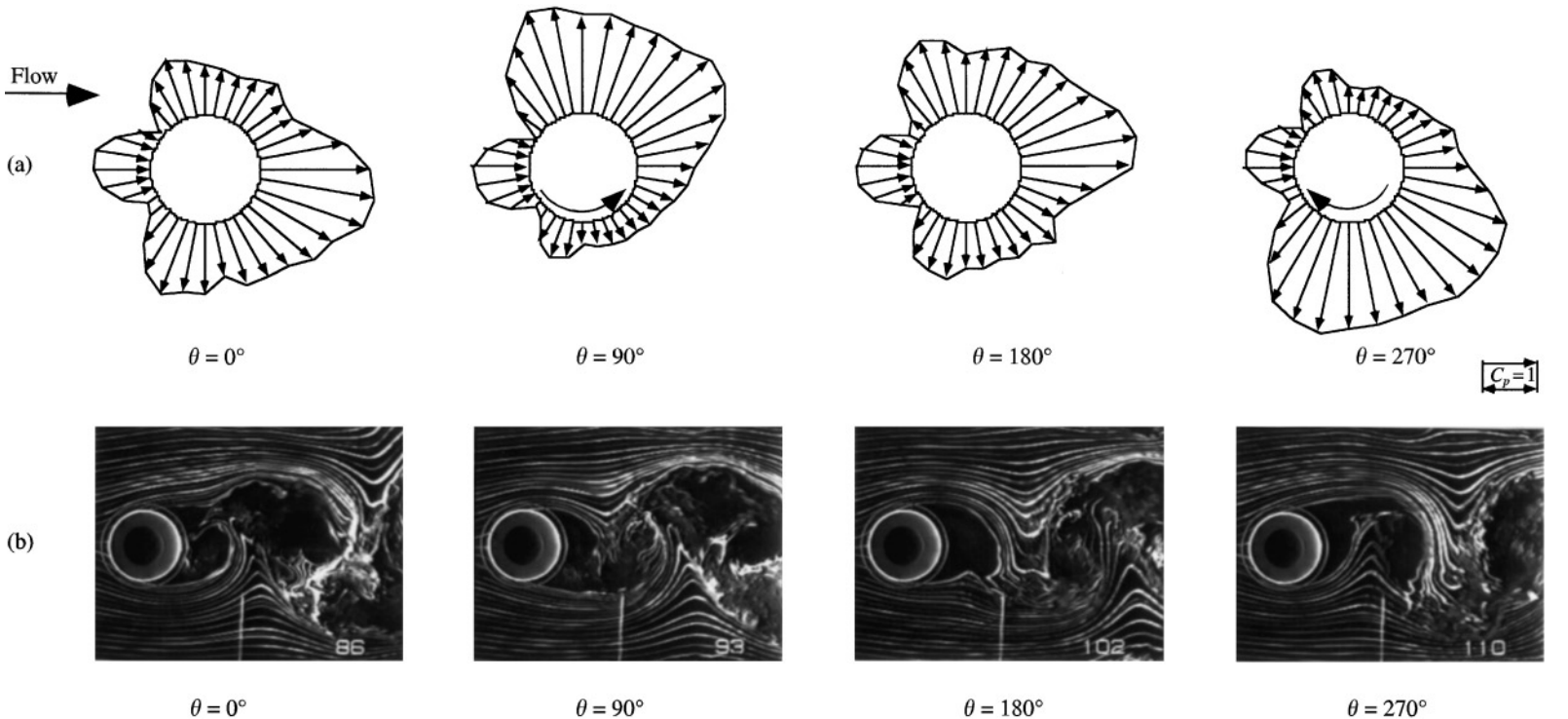

Figure 9. Pressure distributions and visualized flow fields around a rotationally oscillating cylinder at peak resonance with small oscillation amplitude ($S_r = 0{\cdot}19$, $V_r = 0{\cdot}19$): (a) pressure distributions; (b) flow visualizations.

forcing Strouhal number is $S_r = 0{\cdot}19$ and with a small oscillation amplitude of $V_r = 0{\cdot}19$. A large deflection of the cylinder wake appears at the oscillation angles of $\theta = 90^\circ$ and 270°. At the oscillation angle $\theta = 90^\circ$, the cylinder wake is deflected downward by the appearance of roll-down vortex motion over the top surface, which induces a negative pressure, as shown in the measured pressure distributions; while, the flow over the bottom surface of the cylinder is relaxed and the recovery in the surface pressure occurs. On the other hand, upward deflection of the cylinder wake appears at the oscillation angle $\theta = 270^\circ$, and hence a roll-up motion with pressure decrease occurs over the bottom surface and the flow relaxation with pressure recovery appears over the top surface. Similar relations of the pressure distributions and the flow patterns are observed at the other oscillation angles, $\theta = 0$ and 180°. Therefore, the variations of the pressure distributions over the cylinder surface are consistent with the flow pattern variations in the cylinder wake, which has been observed in Figure 8. On the other hand, the rotating direction of the cylinder is not consistent with the variations of flow pattern and pressure distributions. The opposite effect will be expected when the circular cylinder rotates in steady rotary motion [e.g., Swanson (1961)]. The present result suggests that there exists a phase lag of about 180° between the cylinder oscillation and the flow at vortex shedding resonance.

Figure 10 shows the pressure distributions and the corresponding flow visualization pictures of the rotary oscillating cylinders in vortex shedding resonance, where the forcing Strouhal number is $S_r = 0{\cdot}17$ and with large oscillation amplitude of $V_r = 0{\cdot}38$. It is clear that the magnitude of roll-up motion and the consequent formation of a vortex is strengthened in comparison with the small oscillation amplitude of $V_r = 0{\cdot}19$ in Figure 9. The increase in vortex size suggests a reduction in the forcing Strouhal number with an increase in oscillation amplitude at peak vortex shedding resonance, as shown in Figure 5. On the other hand, the pressure distributions over the cylinder surface are modified, reflecting the effect of oscillation amplitude. The pressure distributions at $\theta = 0^\circ$ show a similar behavior as those over the small amplitude oscillations between $\theta = 0^\circ$–90° in Figure 9, suggesting the phase advance about 45° with an increase in oscillation amplitude, which has been observed in Figure 7. A similar trend of phase advance appears in other pressure distributions and the flow visualization pictures. It should be mentioned that the negative pressure over the downstream side of the cylinder is strengthened and the roll-up motion of vortex formation is enlarged with an increase in oscillation amplitude, which suggests the cause of phase lag between the cylinder oscillation and the flow around the cylinder under resonance conditions.

Figure 11 shows the mean drag C_D and root-mean-square lift coefficient $C_{L\mathrm{rms}}$ in relation to the Strouhal number at the large oscillation amplitude $V_r = 0{\cdot}38$. These coefficients are estimated from the phase-averaged drag and lift coefficients measured at various vortex angles ϕ, as shown in Figures 7 and 8. It is clear that both coefficients show peaks around $S_r = 0{\cdot}17$, which indicates that the vortex shedding resonance also appears in the fluid forces similarly to the measured velocity fluctuations in Figure 5. It can be seen that the mean drag and root-mean-square lift coefficients under the non-resonant condition are even larger than those of the stationary cylinder. Hence, the present result indicates that the simple rotary oscillation in the range of $S_r = 0$–$0{\cdot}22$ and at $V_r = 0{\cdot}38$ (maximum oscillation angle $\theta_{\max} = 35^\circ$) does not reduce the drag force acting on the cylinder in comparison with the stationary cylinder. This result is different from the observation by Tokumaru and Dimotakis (1991), who observed the drag reduction by rotary oscillation at much larger oscillation amplitude, $V_r = 2$ ($\theta_{\max} = 180^\circ$). It is expected that the drag on the cylinder is strongly dependent on the oscillation amplitude as well as on the forcing Strouhal number. However, both results show similar trends of a decrease in the drag coefficient with an increase in forcing Strouhal numbers in the range of $S_r = 0{\cdot}17$–$0{\cdot}22$.

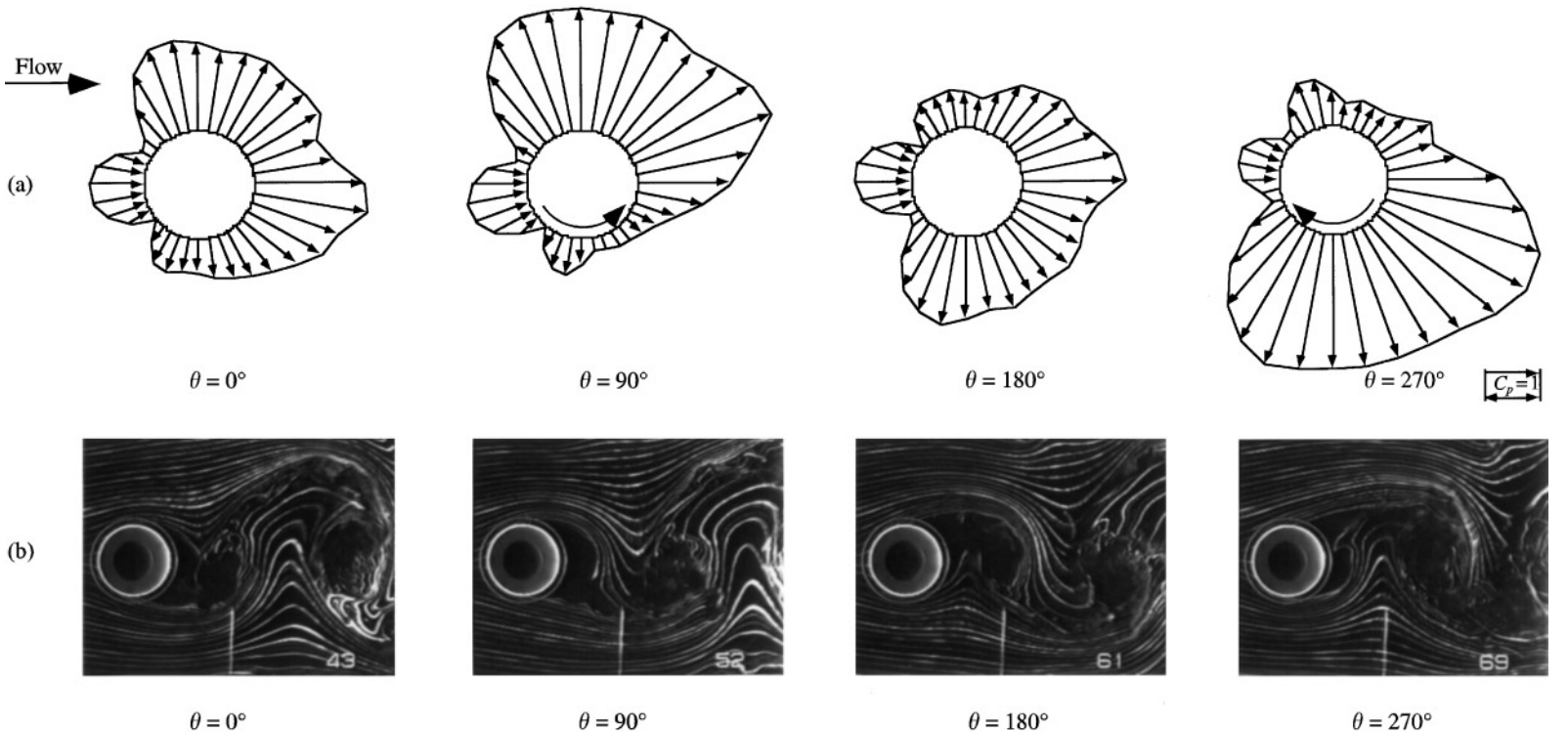

Figure 10. Pressure distributions and visualized flow fields around a rotationally oscillating cylinder at peak resonance with large oscillation amplitude ($S_r = 0{\cdot}17$, $V_r = 0{\cdot}38$): (a) pressure distributions; (b) flow visualizations.

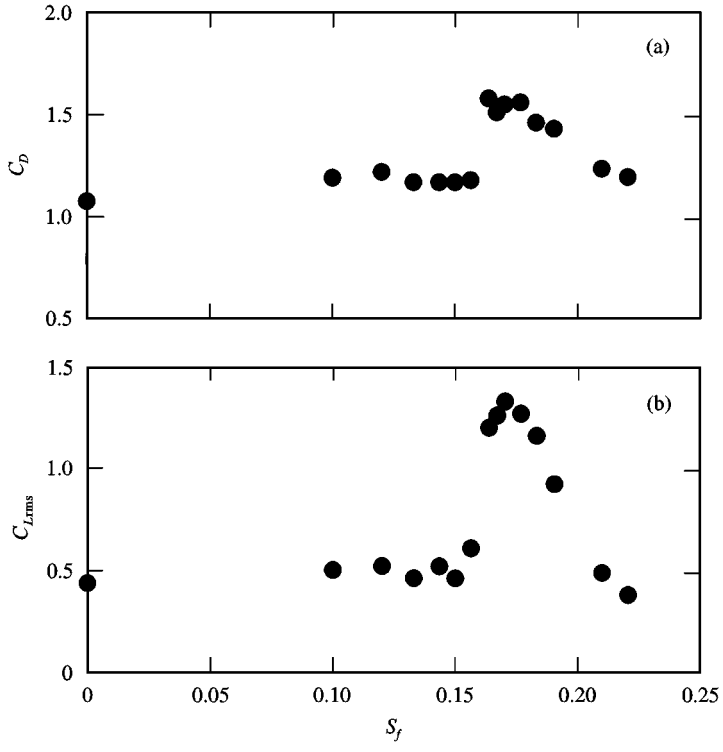

Figure 11. Mean drag and root-mean-square lift coefficients with respect to the forcing Strouhal number ($V_r = 0{\cdot}38$): (a) mean drag coefficient; (b) r.m.s. lift coefficient.

4. CONCLUSIONS

The vortex shedding resonance of a circular cylinder wake to forced rotational oscillations has been investigated by measuring the velocity fluctuations in the wake and the pressure distributions over the cylinder surface. The velocity fluctuations in the cylinder wake and the phase-averaged drag and lift forces acting on the cylinder are strengthened near the natural frequency of vortex shedding at small-amplitude oscillation, while the peak resonance frequency shifts to a lower value with increasing oscillation amplitude. The variations of drag and lift forces with the oscillation angles indicate that the phase lag of fluid forces to the cylinder oscillation increases with the growth of oscillation amplitude and forcing Strouhal number, supporting the observations on the variation of peak resonance frequency with oscillation amplitude.

The comparative study of the measured pressure distributions and the simultaneous flow visualization with respect to cylinder rotation shows that the vortex formation is strengthened and the pressure distributions over the cylinder surface are modified, which eflects the mechanism of decrease in peak resonance frequency with an increase in oscillation amplitude. It is also found that the variations of surface pressure distributions are consistent with the flow-pattern variations, but there is a phase between the cylinder oscillation and the flow field under resonance conditions.

References

Bearman, P. W. 1984 Vortex shedding from oscillating bluff bodies. *Annual Review of Fluid Mechanics* **16,** 195–222.

DRESCHER, H. 1956 Messung der auf querongestromte Zylinder ausgeubten seitlich veranderten Drucke. *Zeitschrift für Flugwissensschaft* **4,** 17–21.

FILLER, J. R., MARSTON, P. L. & MIH, W. C. 1991 Response of the shear layers separating from a circular cylinder to small-amplitude rotational oscillations. *Journal of Fluid Mechanics* **231,** 481–499.

FUJISAWA, N. & KAWAJI, Y. 1995 Active control of vortex shedding from a circular cylinder by rotary oscillations. In *Proceedings 10th Symposium on Turbulent Shear Flows*, University Park, PA, U.S.A., pp. 14.25–14.30.

GRIFFIN, O. M. & HALL, M. S. 1991 Review: Vortex shedding lock-on and flow control in bluff body wakes. *ASME Journal of Fluids Engineering* **113,** 526–537.

KING, R. 1977 A review of vortex shedding research and its application. *Ocean Engineering* **4,** 141–172.

NAUDASCHER, E. 1987 Flow-induced streamwise vibrations of structures. *Journal of Fluids and Structures* **1,** 265–298.

OKAJIMA, A. TAKATA, H. & ASANUMA, T. 1975 Viscous flow around a rotationally oscillating circular cylinder. *Reports of Institute of Space and Aeronautical Science*, University of Tokyo, No. 532, pp. 311–338.

TANEDA, S. 1978 Visual observations of the flow past a circular cylinder performing a rotary oscillation. *Journal of the Physical Society of Japan* **45,** 1038–1043.

SWANSON, W. M. 1961 The Magnus effect: a summary of investigations to date. *ASME Journal of Basic Engineering* **83,** 461–470.

TOKUMARU, P. T. & DIMOTAKIS, P. E. 1991 Rotary oscillation control of a cylinder wake. *Journal of Fluid Mechanics* **224,** 77–90.